

Cite this: *Chem. Sci.*, 2019, **10**, 6368 All publication charges for this article have been paid for by the Royal Society of ChemistryReceived 12th April 2019  
Accepted 19th May 2019DOI: 10.1039/c9sc01818b  
[rsc.li/chemical-science](http://rsc.li/chemical-science)

## 1. Introduction

The sulfonamide group,  $\text{SO}_2\text{NHR}$ , is an acidic moiety that features heavily in pharmaceutical and agrochemical compounds, yet is surprisingly uncommon in nature. ZINC, a database commonly used in virtual screening, listed 4781 commercially available derivatives of methylsulfonamide in 2016.<sup>1</sup> There are  $\sim 200$  sulfonamide-containing drugs currently on the market.<sup>2</sup> Examples include antibiotics, anti-glaucoma,<sup>3</sup> diuretics, anticonvulsants, antidiabetics and anti-cancer agents.<sup>4–6</sup> Due to the prevalence of this group in the design of modern bioactive compounds, research into optimized methods for their synthesis continues to be of relevance.<sup>7–9</sup> Sulfonamide antibiotics (SAs) were the first widely used antibiotic agents, and arguably paved the way for the antibiotic revolution. Their antibacterial action stems from the competitive inhibition of *p*-aminobenzoic acid in the folic acid metabolism cycle, which prevents bacterial multiplication. It is

estimated that after administration, 30–90% of SAs are excreted either as the parent compound, or as acetic acid conjugates.<sup>10</sup> Recent reports suggest that the environmental pollution caused by such widespread historical usage of SAs and other antibiotics may pose harmful effects to aquatic organisms.<sup>11</sup> Further risk to human health may also arise from their prevalence in the food chain *via* the soil environment.<sup>12</sup>

The acid dissociation constant,  $K_{\text{a}}$ , defines the extent to which dissociation of a proton is thermodynamically feasible at a given pH. It provides a means to rationalize acid–base activity in aqueous conditions, an insight that is fundamental to numerous areas of chemistry and biochemistry. Approaches to  $pK_{\text{a}}$  prediction may be classified as either “first principles” or “empirical”. Purely first-principles methods access the  $pK_{\text{a}}$  value *via* the calculation of  $\Delta G$  for dissociation, using the van’t Hoff’s isotherm to calculate the dissociation constant. The broad applicability of this approach makes it attractive, and it has been explored using many quantum mechanical approaches.<sup>13–18</sup> However, the significant CPU-time that electronic structure calculations incur remains a detriment to the utility of this approach in larger scale screening studies. The program “Jaguar  $pK_{\text{a}}$ ” by Schrödinger is the only commercially available first-principles base  $pK_{\text{a}}$  prediction package.<sup>19,20</sup> The second widely explored approach is to construct an empirically derived model based on the relationships between various

<sup>a</sup>Manchester Institute of Biotechnology (MIB), 131 Princess Street, Manchester M1 7DN, UK. E-mail: [pla@manchester.ac.uk](mailto:pla@manchester.ac.uk)

<sup>b</sup>School of Chemistry, University of Manchester, Oxford Road, Manchester M13 9PL, UK

<sup>c</sup>Syngenta AG, Jealott’s Hill, Warfield, Bracknell, RG42 6E7, UK

† Electronic supplementary information (ESI) available. See DOI: [10.1039/c9sc01818b](https://doi.org/10.1039/c9sc01818b)



chemical descriptors and experimental  $pK_a$  data. The programs Marvin<sup>21</sup> (ChemAxon), Epik<sup>22</sup> (Schrödinger), and “Classic” and “GALAS” of ACD Labs<sup>23</sup> are just some examples of commercially available packages, all of which implement variants of an empirical-based workflow. Other recent empirical approaches have implemented machine learning methods such as artificial neural nets<sup>24</sup> and support vector regression.<sup>25</sup>

Philipp *et al.* recently highlighted several issues that remain relevant to both first-principles and empirical-based communities.<sup>20</sup> Firstly, the use of 2D molecular representations (*e.g.* SMILES or SMARTS strings), can lead to poor predictions for compounds with  $pK_a$  values strongly influenced by geometric features. For example, steric effects, or stereospecific hydrogen bonding interactions, can affect the thermodynamic feasibility of dissociation. Whereas these effects must be explicitly parameterized using 2D structures, the problem becomes less pronounced in first-principles approaches due to the use of 3D geometries. Another problem highlighted by Philipp *et al.* is the case of tautomerizable compounds. A theoretically rigorous quantum mechanical approach requires the generation of an ensemble of low-lying conformations for each tautomeric state. This increases computation times, a problem further enhanced in the case of *multiprotic* tautomerizable compounds. For empirical approaches the problem with tautomerism arises with the need to recognize the dominant tautomeric state, owing to the fact that different tautomers may have different  $pK_a$  values. Experimental evidence in support of tautomeric preference is lacking for many species.<sup>26,27</sup>

Strikingly well-defined linear relationships between bond lengths and  $pK_a$  have now been shown to emerge for many functional groups.<sup>28–33</sup> The bond length allows for the partitioning of chemical space into subsets of compounds, within which the site of ionization shares a specific local chemical environment. In the current work, we demonstrate for the first time that linear relationships exist between bond lengths of three variants of the sulfonamide group and their propensity to ionize in aqueous conditions. Fig. 1 shows the common skeletons of the training sets and their corresponding target drugs for the three classes of sulfonamides studied: primary benzene sulfonamide derivatives, 4-amino-N-phenylbenzenesulfonamides and phenylsulfonylureas. We then show how these relationships may be exploited to predict  $pK_a$  values of sulfonamide groups on a number of pharmaceutically relevant compounds. We also pose solutions for the more complex issues in  $pK_a$  prediction by demonstrating how to predict with excellent accuracy for (i) multiprotic compounds, (ii) compounds containing more than 50 atoms, and (iii) those compounds that tautomerize. Furthermore, we add credence to the notion that AIBL models (AIBL = Ab Initio Bond Lengths) providing accurate predictions may be established for *any* type of ionizable group, given that some experimental data are available for parameterization.

## 2. Computational methods

### 2.1 Conformational search

Geometries of all stationary points were optimized at B3LYP/6-311G(d,p) level using GAUSSIAN09 with tight convergence

criteria, in both gas and solvent phase using CPCM. Vibrational analysis was then performed at the same level to confirm the nature of the stationary points. For primary benzene sulfonamides (Pr-BSA, Set 1 or S1), two input structures were generated for each compound of the training set (S1-1 to S1-22, listed in Tables S1–S4 in the (ESI<sup>†</sup>)): an *anti*-conformer and a *syn*-conformer, where the labels *anti* and *syn* denote the orientation of the nitrogen lone pair relative to the C–S bond of the sulfonamide fragment. For the 4-amino-N-phenylbenzenesulfonamide (AP-BSA, Set 2 or S2) training set (labelled S2-1 to S2-38, and listed in Tables S5 and S6 of the ESI<sup>†</sup>), the most stable conformation of 4-amino-N-phenylbenzenesulfonamide was identified from an ensemble of 15 optimized geometries by a comparison of total energies. This geometry was then used as the common 3D skeleton for the construction of the remaining 37 S2 analogues. The same method of generating low-lying conformations for the common fragment was used for the third and final series, the sulfonylureas set (SU, Set 3), which contains compounds SU-1 to SU-30, listed in Tables S7–S9.<sup>†</sup> For compounds with flexible substituent groups, several starting geometries were generated for all cases *via* manual rotation around bonds of the substituent group, whilst the sulfonamide group was left unchanged.

For test set compounds TS1-1 to TS1-10 (listed in Results section and in Tables S10–S14<sup>†</sup>), a conformational search was performed *via* use of the “Conformers” plug-in within the MarvinSketch program (version 16.1.4.0) by ChemAxon.<sup>21</sup> A total of 25 conformers were generated using the Dreiding force-field, with diversity threshold and time step set to default. Each conformer was optimized at the B3LYP/6-311G(d,p) level in the gas-phase using GAUSSIAN09 with tight convergence criteria. The most stable geometry of the compound, whilst keeping the *syn* conformation of the sulfonamide group, was then identified by a comparison of total energies. For compounds with more than one site of ionization, the proton at the most acidic site of ionization ( $-\text{SO}_2\text{N}-\text{H}^-$  for TS1-7 to TS1-11 and COO-H for TS1-12 to TS1-14) was removed and the anionic state was also optimized. Optimizations were performed with both the 6-311G(d,p) and 6-311+G(d,p) basis sets. The geometries of the *N*-heterocyclic arenesulfonamide (NHAS) test set compounds labelled TS2-1 to TS2-10 (listed later in the text and in Table S15<sup>†</sup>), were once again obtained *via* selection of the most stable from a conformational ensemble of 25, after optimization using GAUSSIAN09. For the sulfonylureas of the test set, denoted TSU, the compounds glibenclamide, glimepiride and glipizide (listed in Table S16<sup>†</sup>), the number of constituent atoms exceeds 50, and they have a number of rotatable bonds in the R1 and R2 groups. To identify the most stable geometry for each species, a conformational ensemble of 30 geometries was generated using Marvin for each TSU compound, once again followed by optimization using GAUSSIAN09. The above procedure was performed both in gas-phase and with the CPCM, in all cases.

### 2.2 Experimental data

Experimental data were procured from several different literature sources and are referenced throughout the text and in the ESI.<sup>†</sup> All  $pK_a$  values correspond to measurements taken as close



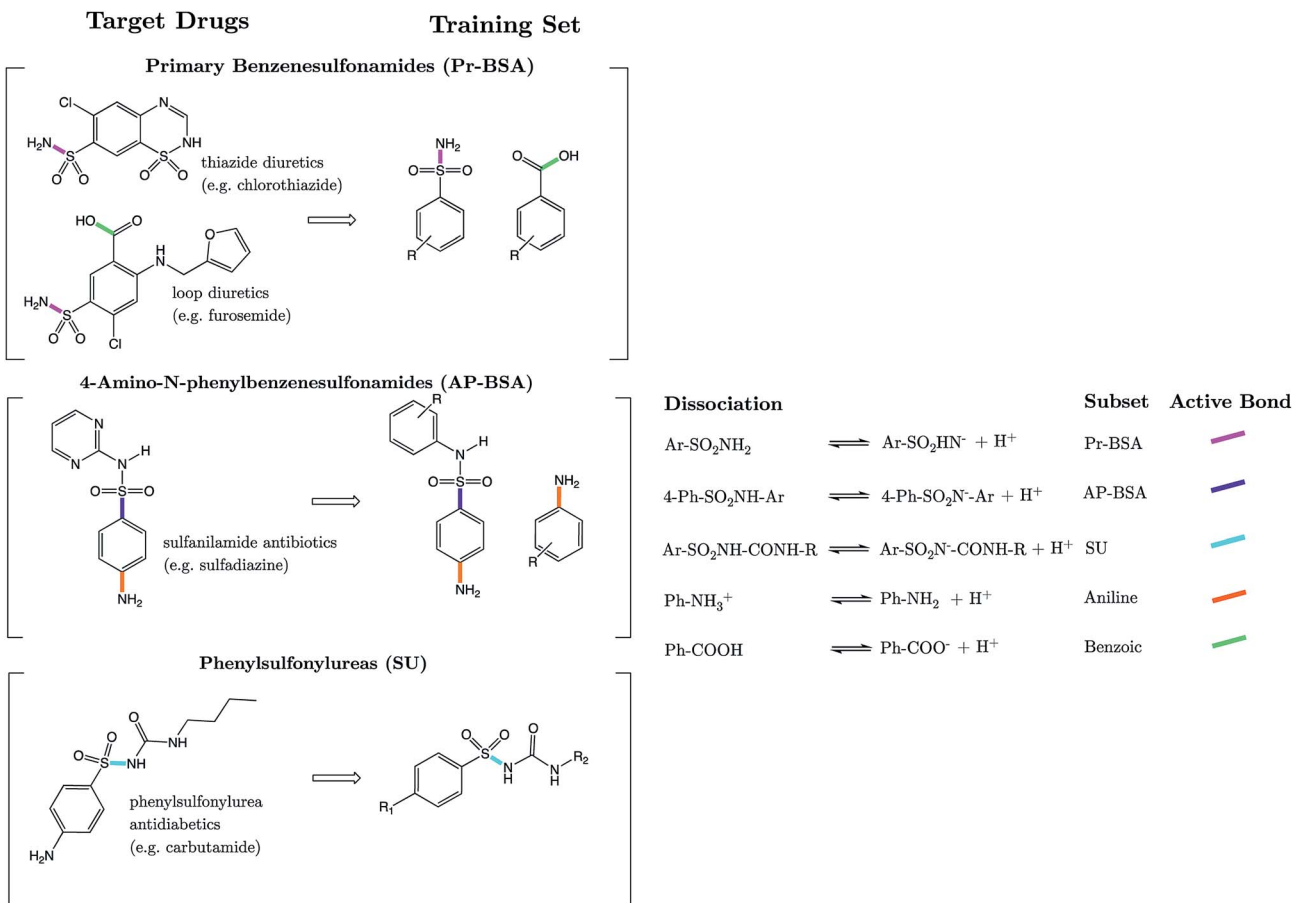


Fig. 1 (Left column) "Target Drugs" are examples of the drug molecules we target in this work. (Right column) "Training set" shows the common substructure of the sets of analogues used to form the models. Active bonds identified and used later in predictive equations are shown in a bold colour.

to standard conditions as possible, *i.e.* 298.15 K and 1 atm. The new values for celecoxib, glimepiride and glipizide were measured in this work using the SiriusT3 instrument, an automatic titration system incorporating *in situ* UV spectroscopy. More details of experimental measurements are given in Technical Section 1 of the ESI.†

### 2.3 Model validation

Each of the three subgroups studied here consist of a series of closely related analogues of benzene sulfonamide (**S1-1** to **S1-22** and **TS1-1** to **TS1-14**, a total of  $22 + 14 = 36$  compounds), 4-amino-N-phenylbenzenesulfonamides (**S2-1** to **S2-38** and **TS2-1** to **TS2-10**, a total of  $38 + 10 = 48$  compounds) and phenylsulfonylurea (**SU-1** to **SU-30** and **TSU-1** to **TSU-6**, a total of  $30 + 6 = 36$ ). Each of the three subsets was analyzed separately for the existence of linear relationships between bond lengths close to the site of ionization and  $pK_a$ . Ordinary least-squares regression was performed and assessment goodness-of-fit was performed using the squared correlation coefficient ( $r^2$ ) and the Root-Mean-Squared-Error of Estimation (RMSEE). Cross validation was performed by calculation of the leave-one-seventh-out  $q^2$  value using the program SIMCA-P,<sup>34</sup> to give some

estimation of model predictability. The equations defining these metrics can be found in Technical Section 2 of the ESI,† in addition to Mean Absolute Error (MAE)-based criteria that Roy has recommended<sup>35</sup> for evaluation of QSAR/QSPR models.

### 2.4 IQA calculations

In the Discussion section, the trend in bond length variation with  $pK_a$  is analysed to derive a rationale for the origins of each relationship. The energy decomposition framework called Interacting Quantum Atoms (IQA)<sup>36</sup> was used *via* the program AIMall (version16.01.09) to derive quantities describing the extent of delocalization between atoms, and the electrostatic interaction between atoms, respectively. Details of this procedure can be found in Technical Section 3.

## 3. Results

### 3.1 Models: primary benzene sulfonamides (Pr-BSAs)

For primary benzene sulfonamides we wish to predict the thermodynamic feasibility of the dissociation  $\text{SO}_2\text{-NH}_2 \rightarrow \text{SO}_2\text{-N}^- \text{H} + \text{H}^+$ . The bond lengths of the sulfonamide group under investigation are shown in Fig. 2a, labelled a-f. Several studies

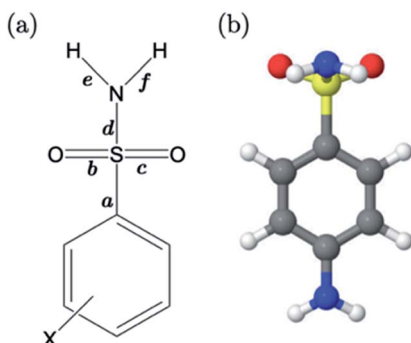


Fig. 2 (a) The common fragment of the Pr-BSA series, where bond lengths under investigation for their relationship with  $pK_a$  are labelled a-f. (b) The dominant (*anti*) conformation of the sulfonamide group in the presence of CPCM, labelled B for sulfanilamide, *i.e.*  $X = \text{NH}_2$ .

concerning the gas-phase conformation of benzene sulfonamide and its derivatives have been performed.<sup>37–39</sup> The general consensus is that two dominant conformations exist for the  $-\text{SO}_2\text{NH}_2$  group, which can be labelled “*syn*” and “*anti*” denoting the orientation of the lone pair on the nitrogen atom relative to the C-S bond (shown in Fig. S1 of the ESI<sup>†</sup>). In this work we use a set of 22 substituted benzene sulfonamides (labelled S1-1 to S1-22 and shown in Tables S1-S4<sup>†</sup>) to construct bond length- $pK_a$  models. For each S1 compound, the *syn* and *anti*-conformers were located (shown in Fig. S1 of the ESI<sup>†</sup>). We find that, in the presence of the CPCM implicit solvation model, the *anti*-conformer (Fig. 2b) is on average  $\sim 4 \text{ kJ mol}^{-1}$  more stable than *syn* across the series.

Results of linear regression of each bond length a-f of the CPCM-solvated structures against  $pK_a$  reveal superior internal validation statistics for the S-N bonding distance ( $r^2 = 0.95$ ,  $q^2 = 0.94$  and RMSEE = 0.14). The full set of statistics for each bond length model can be found in Table S17.<sup>†</sup>

The proximity of an *ortho*-substituent to the sulfonamide group means that it can influence bond lengths of  $\text{SO}_2\text{NH}_2$  *via* steric effects and intramolecular hydrogen bonding interactions, depending on the type of substituent. If the *ortho* compounds are removed, strong ( $r^2 > 0.8$ ), *positive* correlations with  $pK_a$  are observed for *all* bonds except C-S (a), which is *negatively* correlated. That is to say, shorter S=O (b and c), S-N (d) and N-H (e and f) bond distances are indicative of a greater propensity to ionize, whilst the C-S bond becomes longer with increased acidity. These relationships are illustrated in the plots shown in Fig. S2.<sup>†</sup> We note that the nature of the variation in bonding distances a-f is the same for *syn* and *anti*-conformers in both gas and solvent phase. Therefore, the effect that a substituent has on the constituent bond lengths of the ionizable group is reflected in the relative propensity of the molecule to lose a proton. Overall, those compounds with substituents that make the phenyl group more electron-poor exhibit a lower  $pK_a$ , and *vice versa*. In the next section, we make predictions for 14 drug molecules using the equation describing the linear line of best fit for the S-N bond length model, *i.e.*,  $pK_a = 92.95 \times r(\text{S-N}) - 145.10$ .

### 3.2 Predictions: neutral Pr-BSAs

We chose six compounds for the first test set (TS1) which exhibit a  $pK_a$  value corresponding to dissociation of the proton at the sulfonamide group, whilst the rest of the molecule is in a *neutral* state. These six compounds are methyclothiazide (TS1-1), chlorthalidone (TS1-2), sulpiride (TS1-3), celecoxib (TS1-4), metolazone (TS1-5) and polythiazide (TS1-6).

Predictions made using the equation above for the S-N bond (d) solvated model are illustrated in Fig. 3, and listed in Table S18.<sup>†</sup> All compounds are predicted for to within 0.5 units from literature values aside from celecoxib. Our prediction of 9.72 for celecoxib shows an error of  $-1.38$  with respect to the existing experimental value<sup>40</sup> of 11.1. Due to the anomalously large error of our prediction, a new experimental measurement was taken using the UV-metric technique. As celecoxib is poorly soluble in water but readily dissolves in methanol, it was necessary to perform Yasuda-Shedlovsky extrapolation. This procedure delivers a  $pK_a$  value for aqueous conditions from the relationship between  $pK_a$  value and methanol concentration. Details of the experimental procedure are given in Technical Section 1 of the ESI.<sup>†</sup> This treatment returned a new experimental value of 9.525 as the average of four measurements, with a standard deviation of 0.06. This new value is now 0.2 log units from our predicted value of 9.72. *This success shows that AIBL is able to correct for an erroneous experiment.* As the precise conditions of the 11.1 value are unknown, we can only postulate that it was obtained in non-standard conditions. An increase in  $\sim 1.5$  units can most likely be ascribed to the response of the equilibrium to a lower temperature, the presence of another solvent or a higher ionic strength.

The predictions made by the Marvin tool are also very accurate (MAE = 0.34, see Table S18<sup>†</sup>). This is likely due to the prevalence of benzene sulfonamide analogues and accompanying  $pK_a$  data in the literature. However, it should be noted that the correction of the  $pK_a$  value for celecoxib would not have been realized using the Marvin program, because at 10.7, Marvin's value lies closer to original literature value, and has an error of +1.18 when compared to the new value.

### 3.3 Predictions: anionic Pr-BSAs

The next 8 test compounds are shown in Fig. 4. Each compound of this set has at least two sites of ionization, one of which is a primary sulfonamide group. The thiazide drugs (TS1-7 to TS1-11) exhibit a  $pK_{a(1)}$  value in the range 6 to 9,<sup>41</sup> corresponding to dissociation from a tertiary sulfamoyl group in their secondary ring.<sup>42</sup> Compounds TS1-12 to TS1-14, (bumetanide, furosemide and piretanide) all contain primary sulfonamide groups in addition to a more acidic carboxylic acid group ( $pK_{a(1)} \sim 3.5$ ). Therefore, we optimized the anionic forms (carboxylate anion TS1-12 to TS1-14, and sulfonamide anion for TS1-7 to TS1-11), as well as the neutral states in order to assess the effect of protonation state on prediction accuracy. The results shown in Fig. 4 (and Table S19<sup>†</sup>) indicate that representation of each compound in the anionic microstate is necessary for accurate prediction of their  $pK_a$  values. This assertion is illustrated by a marked decrease in MAE from 0.87 to 0.33 log units for



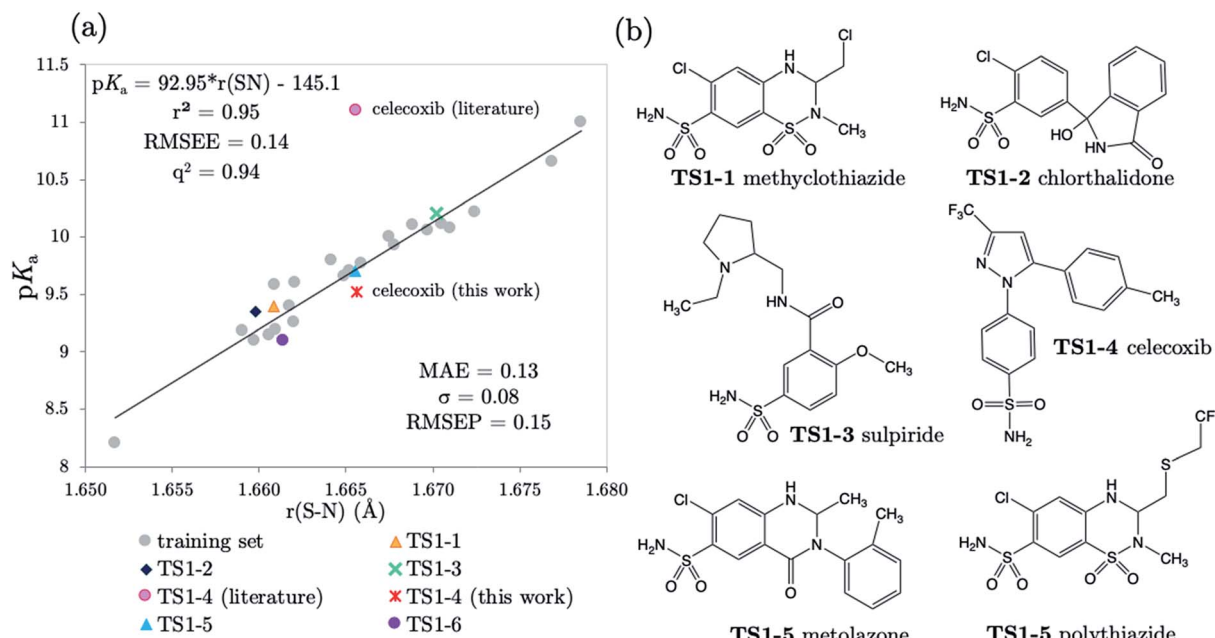


Fig. 3 (a) The relationship between S–N equilibrium bond lengths calculated for the *anti*-conformer using CPCM and  $pK_a$  values for the 22 P-BSA training set compounds, and the equation describing the linear fit; (b) structures of the 6 drug compounds exhibiting a single  $pK_a$  value.

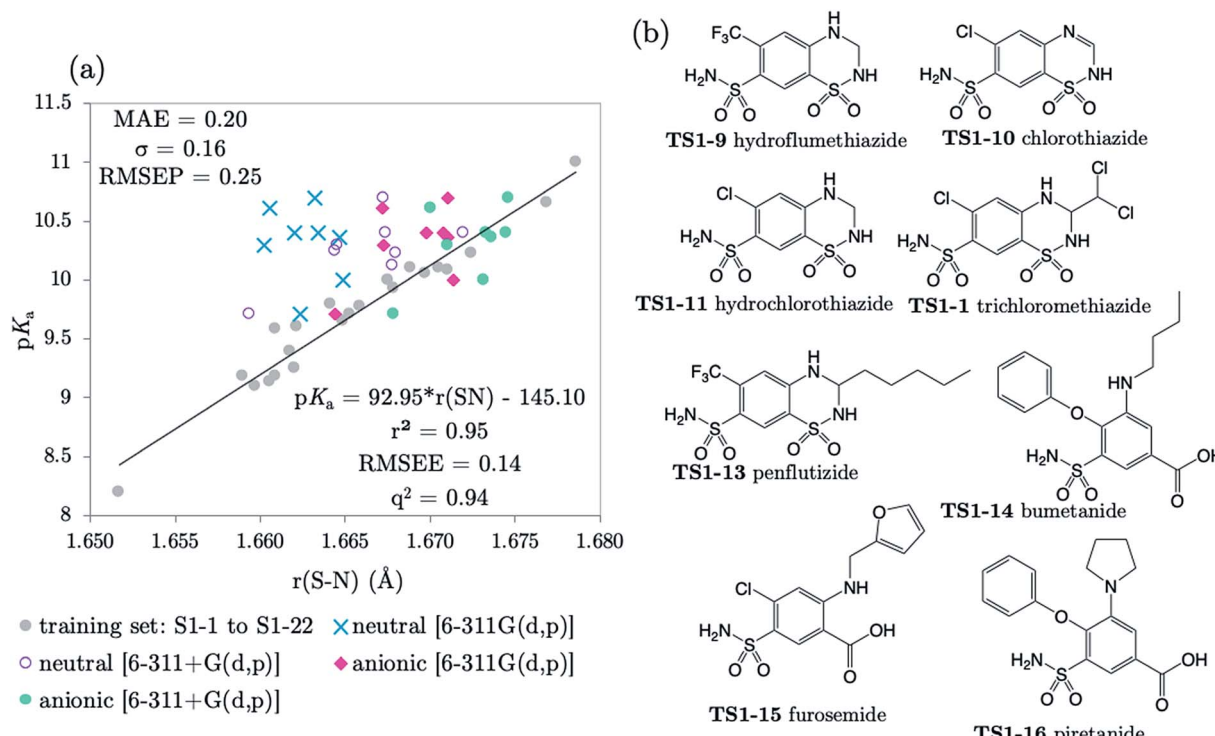


Fig. 4 (a) The relationship between S–N equilibrium bond lengths calculated using CPCM and  $pK_a$  values for the training set S1-1 to S1-22, (gray dots), and the test set, consisting of 8 drug diprotic drug compounds, labelled TS1-7 to TS1-14. SN bond lengths for the test set have been calculated for the neutral state using the 6-311G(d,p) basis set (blue crosses) and the 6-311+G(d,p) basis set (purple circles), the anionic form of each compound using 6-311G(d,p) (pink diamonds) and with the addition of one set of diffuse functions to this basis set [6-311+G(d,p)] (green dots). Bond length values can be found in Tables S11–S14 of the ESI.† (b) Structures of drug compounds TS1-7 to TS1-14. MAE, standard deviation ( $\sigma$ ) and RMSEP shown correspond to the anionic B3LYP/6-311+G(d,p) predictions.

predictions made using the neutral species compared to the anionic state. This improvement (in going from the neutral to the anionic form) is evident even without the inclusion of diffuse functions for non-hydrogen atoms in the basis set. However, inclusion of diffuse functions (6-311+G(d,p)) provides further amelioration of prediction accuracy such that the MAE is reduced to just 0.20, using the SN bond in the anionic form. Allowing distribution of electronic charge over a larger spatial area, *via* the inclusion of diffuse functions, should provide a more accurate description of the diminished electron repulsion at the anion. Thus, we can expect to obtain a better representation of electron distribution near to the active bond site, more accurate bond lengths and greater prediction accuracy. To avoid the lack of consistency the whole training set could be re-optimized with 6-311+G(d,p), rather than just the set of anionic species. However, as the approach taken delivers excellent predictions, this was not deemed necessary.

The applicability radius of this primary sulfonamide model is wide: it covers *ortho*-, *meta*- and *para*-substitution and may be used to predict  $pK_a$  values of sulfonamide groups on diprotic compounds. Whilst the performance of Marvin is still good, with an overall MAE of 0.65, a standard deviation of 0.41 and a RMSEP of 0.82, 4 out of the 16 predictions showed errors of more than 1 log unit and 4 others were between 0.5 and 1 log unit. Furthermore, for 3 out of 5 thiazides (TS1-7, TS1-9 and TS1-11), Marvin predicts that the primary sulfonamide group is more acidic than the tertiary sulfamoyl group. No AIBL- $pK_a$  errors exceeded 0.34 log units, and the trend in  $pK_a$  values across the series from TS1-7 to TS1-14 mirrors that of the experimental values remarkably well, as shown in Fig. 5. Technical Section 4 of the ESI<sup>†</sup> also details how the model passes Roy's MAE-based evaluation criteria.

Taking the *ipso* carbon as the atom bound to the carboxylic acid group, compounds TS1-12, TS1-13 and TS1-14 can be classed as *meta*- and *para*- (*m/p*) substituted benzoic acids. Previous work showed that the gas-phase C–O bond (in the COOH fragment) of *m/p* substituted benzoic acids is positively correlated to aqueous  $pK_a$  (as is the C=O bond distance, whilst the C–C and O–H distances instead show a negative correlation). Using the  $pK_a$  data collated in our previous publication,<sup>28</sup> 41 compounds were re-optimized in the gas-phase at the B3LYP/6-311G(d,p) level of theory. The results previously obtained at the HF/6-31G(d) level were corroborated: the C–O bond length model has an  $r^2$  of 0.90 with  $pK_a$  values. The equation describing this relationship ( $pK_a = 144.97 \times r(\text{C–O}) - 192.56$ ) was used to predict the  $pK_a$  values for the carboxylic acid group, modelled in its neutral form, using the most stable gas-phase conformers identified for TS1-12 to TS1-14. According to the literature, bumetanide, furosemide and piretanide exhibit  $pK_{a(1)}$  values of 3.74,<sup>43</sup> 3.64<sup>44</sup> and 4.00.<sup>45</sup> Our model predicts values of 3.47, 3.33 and 4.23. Whilst it is true that the accurate prediction of  $pK_a$  values for benzoic acid derivatives is no longer considered a challenge for existing methodologies, (although Marvin predicts values of 4.69, 4.26, 4.68), it is pleasing to note that we return an excellent level of accuracy. Furthermore, the relative order of acidity between compounds is predicted correctly by our model.

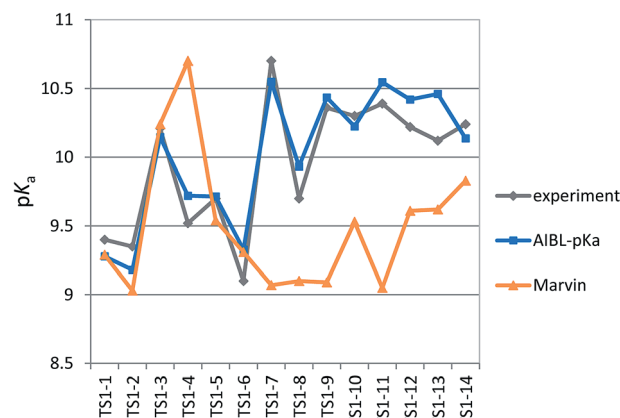


Fig. 5 Relative  $pK_a$  values of the primary sulfonamide group across the series TS1-1 to TS1-14. Although Marvin's performance in terms of mean absolute error evaluation is good (0.65), AIBL- $pK_a$  manages to closely match the overall trend in the magnitude of  $pK_a$  values across the series.

### 3.4 Models: 4-amino-N-phenylbenzenesulfonamides (AP-BSA)

Several drugs have been identified by the derivatization of sulfanilamide with an aromatic group at the N<sup>1</sup> position (denoted "Ar" in Fig. 6a). For such compounds, the influence of the electron-withdrawing arene group causes a general increase in acidity of the  $-\text{SO}_2\text{NH}-$  proton relative to primary sulfonamides. This decrease in  $pK_a$  value means that in aqueous conditions many of these drugs are ionized at physiological pH. One class of secondary sulfonamides which have found widespread usage as therapeutics are *N*-heterocyclic arenesulfonamides (NHAS). For these species, the aryl group contains a heteroatom at the 2-position, allowing them to exhibit sulfanilamide–sulfanilamide tautomerism (Fig. 6b). It is suggested that both tautomeric forms may be important for their therapeutic activity. A recent study<sup>46</sup> by Chourasiya *et al.* has looked specifically at tautomeric polymorphism for a series of sulfanilamide drugs. By comparing gas-phase free energies of the amide and imide forms, they noted that compounds with an N<sub>1</sub>-2- or N<sub>1</sub>-4-pyridyl group preferred the amide state. Their calculations, carried out with an implicit model representing a DMSO environment, suggested that the stability of the imide form is heightened in the presence of a polar solvent. In this work we focus on the sulfonamide form of each S2 and TS2 species only because, based on previous work for guanidines,<sup>33</sup> we expect optimal correlations to emerge using bond lengths of the most stable tautomeric form.

The use of the CPCM implicit solvation model in our geometry optimization for compounds S2-1 to S2-38 provides a marginally superior goodness-of-fit over gas-phase geometries, as measured by  $r^2$  (see Table S20<sup>†</sup>). The C–S bond may be referred to as the most "active bond", as it exhibits the highest  $r^2$  value, at 0.96. The cross-validation  $q^2$  value, which gives an estimate of model predictivity, is also impressively high for C–S at 0.95 and the RMSEE is respectable at 0.23 log units. For S2, the sign of the S–N (iv) slope is negative whilst bonds i, ii, iii, v



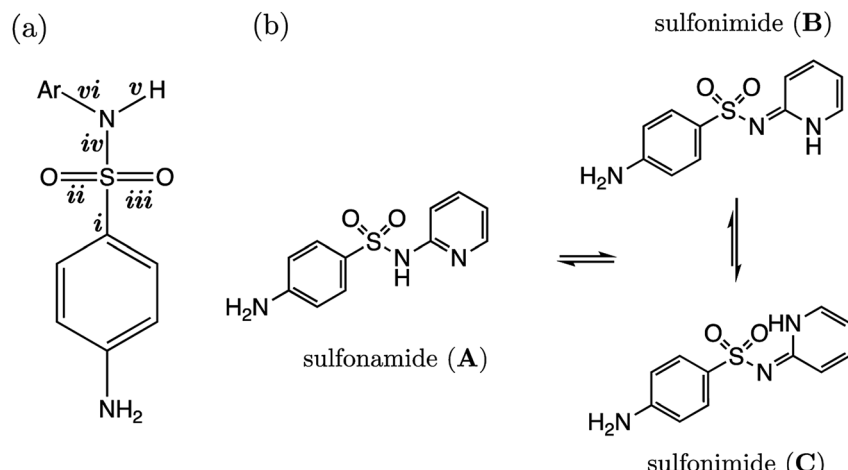


Fig. 6 (a) Common fragment of all sulfonilamides considered as part of the S2 (AP-BSA) reaction series with studied bond lengths labelled i–vi; (b) two tautomeric forms are available to 4-amino-N-(2-pyridyl)benzenesulfonamides (NHAS), which are shown as sulfonamide (A), and the two conformational isomers of the same tautomer, sulfonimides (B) and (C).

and vi have a positive correlation. For this series, the most acidic compound is the 2-Br, 4-NO<sub>2</sub> derivative (labelled S2-37,  $pK_a = 5.7$ ), whereas the least acidic species is the 4-NH<sub>2</sub> derivative (labelled S2-9,  $pK_a = 10.22$ ). We therefore find that the most acidic species in the series has the longest S–N bond (iv), and the shortest C–N bond (vi).

The presence of the *p*-amino group on sulfonilamide means there is an additional microdissociation reaction  $\text{NH}_3^+ \rightarrow \text{NH}_2 + \text{H}^+$ , which has a  $pK_a$  value of  $\sim 2$ . For the sulfonamide group dissociation, the relevant state is the neutral state of each compound. Therefore, the relevant microstate for the aniline group dissociation is the protonated state. However, here we use the neutral state of the compound in accordance with work by Harding *et al.*, which illustrated how there is a linear relationship between  $r(\text{C}-\text{N})$  and  $pK_a$  values for aniline derivatives in the conjugate base form. The variation in C–N bonding distance with  $pK_a$  across a congeneric series can be attributed to the varying extent of  $\text{sp}^2$  hybridization of the nitrogen atom, which is influenced by phenyl substituent groups. For example, in the work of Harding *et al.*, the C–N, and both N–H bonds have a positive correlation with  $pK_a$ , *i.e.*, a shorter bond length (in the presence of *ortho* and *para* electron-withdrawing substituents) corresponds to a lower  $pK_a$ . This bond-shortening effect, coupled with an increase in trigonal planarity, is indicative of a higher degree of  $\text{sp}^2$  character of the nitrogen atom as the phenyl ring becomes more electron-poor at the *ipso* carbon. Enhanced, substituent-induced nitrogen  $\text{sp}^2$  hybridization provides greater resonance stabilization of the neutral conjugate base form. However, a more electron-poor *ipso* carbon destabilizes the conjugate (cationic) acid, thereby favouring the dissociation of N<sup>+</sup>–H, and thus rationalizing the lower  $pK_a$  measured for such species. In this work, 20 aniline derivatives were optimized at the same level of theory used throughout this work [B3LYP/6-311G(d,p)]. Because previous work by Harding *et al.* showed that gas-phase bond lengths exhibit a strong linear relationship with  $pK_a$ , calculations were also carried out *in vacuo* to minimize CPU time. Predictions were made using gas-

phase C–N bond lengths (of the amine group) of test set compounds TS2-1 to TS2-5 and TS2-9 using the equation  $pK_{a(\text{aniline})} = 141.57 \times r(\text{C}-\text{N}) - 193.51$ , for which the  $r^2$  value for the line of best fit was 0.92.

### 3.5 Predictions: AP-BSA

The  $r(\text{C}-\text{S})/\text{CPCM}$  model ( $pK_a = 323.08 \times r(\text{C}-\text{S}) - 564.02$ ) was tested in the case of 10 NHAS drug compounds, which are labelled TS2-1 to TS2-10, and shown in Fig. 7. Experimental aniline  $pK_a$  values are available for compounds TS2-1 to TS2-5 and TS2-9. Our predictions showed an MAE of 0.34, a standard deviation of absolute errors of 0.26 and a RMSEP of 0.40. All predicted values can be found in Table S21.† Low errors (<0.5  $pK_a$  units) are observed for the sulfonamide group predictions for 6 compounds TS2-1, TS2-2, TS2-4, TS2-8, TS2-9 and TS2-10, indicating that this model *can* be applied to 2-pyridine NHAS compounds. However, in the case of compounds TS2-1 to TS2-5, there are multiple  $pK_a$  values in the literature associated with the sulfonamide group, making it a difficult task to truly discern the accuracy of our model. Fig. 7 was produced by choosing the values that best match our predictions, yet there are still three prediction errors that exceed 0.5 log units: TS2-3 (−0.84), TS2-5 (−0.62) and TS2-7 (−0.63). Without additional re-measurement of experimental values, it cannot be confirmed whether the values we predict are indeed more accurate than the reported experimental values, such as in the case of celecoxib.

Representation of each of the compounds TS2-1 to S2-10 as the higher energy sulfonimide tautomer reveals no relationship between bond length and  $pK_a$  (*i.e.*  $r^2 < 0.5$  for all bonds). Yet, in the sulfonamide state the  $r^2$  value for the test set alone is 0.87. It may be asserted that, given our aqueous-phase experimental observable is related to a structural feature of the sulfonamide state, we provide further corroboration to the work of Chourasia and co-workers, which suggests this state is dominant in aqueous conditions.



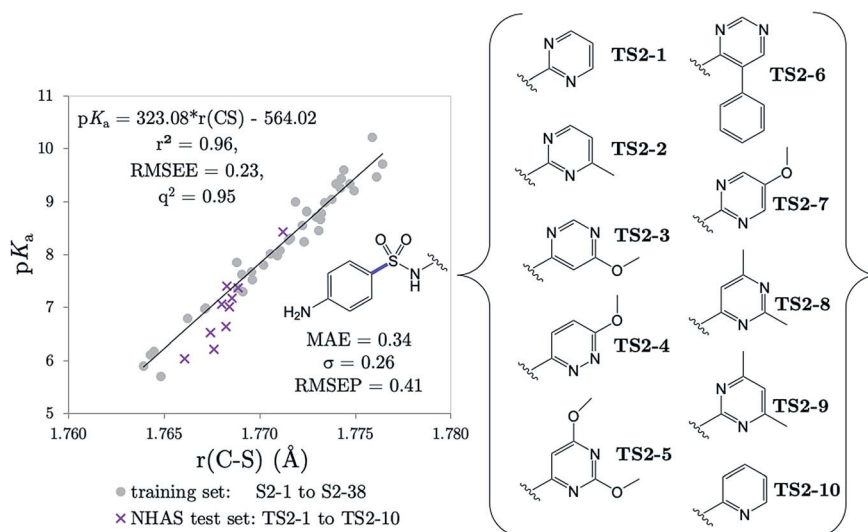


Fig. 7 The relationship between C–S equilibrium bond lengths calculated with CPCM and  $pK_a$  values for our training set (grey dots), and for the 10 NHAS drug compounds (purple crosses), labelled TS2-1 to TS2-10. The C–S equilibrium bond lengths have been calculated using the neutral state of the compound.

Using the same experimental values used to construct Fig. 7, the MAE value for Marvin's predictions is found to be 0.70 with a standard deviation of 0.67. Taking the values closest to Marvin's predictions these values become 0.66 and 0.70. However, the general performance of Marvin is good for this series, and the larger MAE value can be mainly attributed to larger errors for four compounds: TS2-3 (0.93), TS2-6 (0.97), TS2-8 (1.28) and TS2-10 (2.19). A plot showing the general trend across the series for experimental, AIBL- $pK_a$  values and Marvin predictions can be found in Fig. S3 of the SI.<sup>†</sup> Technical Section 5 also details how our model fares according to Roy's MAE-based evaluation criteria for the 14 compounds TS2-1 to TS1-10. The majority of training set data is taken from just one source, where the exact conditions (*i.e.* temperature, solvent) are not reported. It is feasible that the values given in that work were recorded at a temperature lower than 298 K, with a small percentage of another less polar solvent, or at a different ionic strength to the drug compounds. The amalgamation of the test and training set data points returns a linear fit with an  $r^2$  value of 0.95. It may be asserted that the use of this equation, in the case of future predictions may help towards reducing systematic error associated with deviation from standard conditions between test and training set.

### 3.6 Models: sulfonylureas (SU)

The sulfonylurea group is common to many compounds that have been recognized for their biological activities. These include antihypertensive,<sup>47</sup> antineoplastic<sup>48</sup> and antibacterial<sup>49</sup> drugs, in addition to some compounds that exhibit herbicidal action.<sup>50</sup> Notably, sulfonylurea (SU) drugs have been used extensively in the treatment of non-insulin dependent diabetes mellitus. Antidiabetic SU drugs may be broadly classified into first, second or third generation, where second and third generation SU drugs generally require smaller dosage, and

provide a longer action than first generation analogues. First generation drugs contain a central phenylsulfonylurea fragment, with a small *para*-substituent on the phenyl ring. Second and third generation SU drugs have much larger  $R_1$  groups (see groups highlighted in blue in Fig. 8). Due to the influence of the carbonyl group, sulfonylureas are more acidic by 2–4  $pK_a$  units compared to the primary and secondary sulfonamides discussed in the previous sections.

The most recent computational study of sulfonylurea type compounds was carried out by Kasetti *et al.* in 2010.<sup>51</sup> In that work, the authors note that the global minimum conformation of the sulfonylurea fragment, in the gas-phase, contains an N–H···O=S hydrogen bond. The existence of this IHB is corroborated by analysis of bond critical point properties (a concept derived from Atoms in Molecules theory and carried out by the program AIM2000). The iminol tautomeric forms of sulfonylureas were also assessed for their stability relative to the amine form, and were found to be  $\sim$ 21–25 kJ mol<sup>−1</sup> higher in energy. Our working hypothesis is that an AIBL- $pK_a$  model should emerge from the bond lengths of the lowest energy conformations of the lowest energy tautomeric form of our compounds. Therefore, only the amine tautomer form is considered in the following discussion.

The most stable conformation of all 35 compounds of our dataset contain a phenylsulfonylurea fragment, the 3D geometry of which closely resembles that of the optimized structure reported by Kasetti *et al.* This structure is shown in Fig. S3.<sup>†</sup> In the following analysis, we use the 6 marketed drug compounds (shown in Fig. 8) as a test set. With the additional data procured from the literature making up the training set (30 compounds, SU-1 to SU-30 as shown in Table S7<sup>†</sup>), there is a 20/80 split of external test set to training set.

Phenylsulfonylureas are found to have the same active bond length as the Pr-BSA series (S–N), despite the differing chemical environment of the acidic proton (full set of statistics relating to

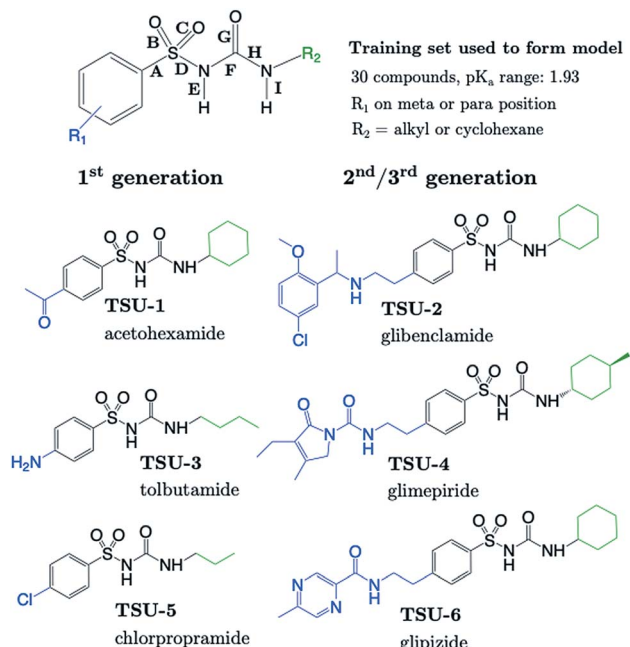


Fig. 8 The generic structure of both training and test set compounds of phenylsulfonylurea (SU) type. Six test compounds were chosen on the basis that they are marketed drug compounds, including 3 first-generation and 3 second-generation SU antidiabetic drugs. R<sub>1</sub> groups are labelled in blue and R<sub>2</sub> groups in green.

each bond length *vs.* p*K*<sub>a</sub> model is shown in Table S22†. Although the *r*<sup>2</sup> and *q*<sup>2</sup> values for the S–N bond (D) model are only 0.93, the RMSEE is particularly low at 0.14. Notably, a relationship emerges here for the S–N bond lengths despite significant variation in the identity of *both* the R<sub>1</sub> and R<sub>2</sub> groups (see Table S7†).

### 3.7 Predictions: SU drugs

Table 1 shows that four out of six SU drugs were predicted to within 0.1 log units from literature experimental values. The largest prediction errors in Table 1 correspond to glipizide and glimepiride. Due to their size and conformational flexibility, a second conformer search (50 input conformers) was carried

out to rule out the possibility that the poor prediction accuracy is due to identification of an incorrect global minimum. The most stable arrangement returned by this second conformer search was found to match that of the first. The low-lying geometries of glimepiride have been discussed a number of times in the literature. The general consensus is that *in vacuo*, a “U-shape” conformation is preferred. However, if hydrogen bonding interactions with a solvent environment were to be modelled explicitly, an “extended” conformation should be favoured. Here, we find that the most stable geometry in both gas and solvent phase (CPCM) is the U-shaped conformation, which at the B3LYP/6-311G(d,p) level, is ~4 kJ mol<sup>-1</sup> more stable than the extended geometry previously identified as most stable by Kasetti.<sup>51</sup> Grbic and co-workers have reported<sup>52</sup> the most recent experimental p*K*<sub>a</sub> value for glimepiride (7.26). In both conformations, the bond length predicts a greater ionization propensity than this value suggests (5.02 for the extended form and 5.58 for U-shaped).

To investigate the cause of these large prediction errors, p*K*<sub>a</sub> values for glimepiride and glipizide were measured once more in this work using the UV-metric method. Measurements were taken in three different methanol concentrations, and p*K*<sub>a</sub> values in aqueous conditions were obtained *via* Yasuda-Shedlovsky extrapolation. The new value for glipizide of 5.21 matches our prediction (5.07) to within 0.14 log units and the new value for glimepiride matches our prediction to within 0.26 log units. Given that our prediction and the new measurement are similar, and given that these two values are also close to those of the structurally similar compounds, glipizide and glibenclamide, we are inclined to believe that 5.32 is the most accurate experimental value for glimepiride.

There is an important consequence of the substantial correction in p*K*<sub>a</sub> value established here. According to the Henderson–Hasselbalch equation, the new p*K*<sub>a</sub> value of 5.32 for glimepiride suggests that 99% of molecules are ionized at pH 7.4 (cell pH), whereas the previously reported value of 7.26 suggests that only 58% are ionized. The therapeutic activity of insulin secretagogues like glimepiride is known to stem from their ability to bind to a receptor on the ATP sensitive K<sup>+</sup> channels of pancreatic β-cell membranes.<sup>58</sup> It is thought that the anionic state of the molecule partakes in this binding

Table 1 S–N bond lengths calculated using CPCM (Å), experimental p*K*<sub>a</sub> values and predictions made using the equation for the S–N/CPCM bond length *versus* p*K*<sub>a</sub> value for 30 analogues: p*K*<sub>a</sub> = 123.194 × *r*(S–N) – 202.904. Values and prediction errors obtained using the Marvin program are also shown, with MAE, σ and RMSEP reported for the lowest prediction errors

ID	Drug	<i>r</i> (S–N)	Exp. p <i>K</i> <sub>a</sub>	AIBL-p <i>K</i> <sub>a</sub>	AE	Marvin	AE
TSU-1	Chlorpropamide	1.68513	4.75 (ref. 53)	4.69	0.06	4.31	0.44
TSU-2	Carbutamide	1.69367	5.79 (ref. 54)	5.75	0.04	4.35	1.44
TSU-3	Acetohexamide	1.68266	4.31 (ref. 54)	4.39	0.08	3.33	0.98
TSU-4	Glibenclamide	1.68980	5.22 (ref. 55)/5.30 (ref. 56)/6.80 (ref. 56)	5.27	0.05/0.03/1.53	4.32	0.90/0.98/2.48
TSU-5	Glipizide	1.68822	5.21 <sup>a</sup> /5.90 (ref. 57)	5.07	0.14/0.83	4.32	0.89/1.58
TSU-6	Glimepiride	1.69235	5.32 <sup>a</sup> /7.26 (ref. 52)/8.03 (ref. 52)	5.58	0.26/1.68/2.45	4.32	1.00/2.94/3.71
MAE							
σ							
RMSEP							

<sup>a</sup> p*K*<sub>a</sub> value measured in this work. All bond lengths for compounds TSU-1 to TSU-6 are given in Table S16 in the ESI.



activity.<sup>59</sup> A higher percentage of molecules existing in their ionized state means that there is a higher percentage that can partake in binding with the receptor to block the channel, which should be linked to greater efficacy of the drug. As glimepiride is currently used in the treatment of diabetes, the lower value that we report is perhaps in better agreement with its known therapeutic effects.

Finally, we note that the use of the S–N bond length of the glimepiride conformer that is likely to be more stable in solution gives a marginally larger error than the most stable gas-phase/CPCM conformation, compared to the new value of 5.32. This perhaps goes against chemical intuition. However, it is pleasing to note that good estimations of  $pK_a$  may be made without user knowledge of explicitly solvated conformational preference, as is almost always the case in practice.

Table 1 shows that the average prediction accuracy of the Marvin program is inferior to that of AIBL for the same compounds, with all but one of the predictions giving an error of more than 0.5 units. Moreover, the Marvin MAE is 0.94 whereas ours is 0.10. Note that Marvin and AIBL have been compared on an equal footing and allowing for their best performance because, for both, we took the experimental values closest to their respective predictions. The trend of experimental  $pK_a$  variation across the test set series is compared to AIBL- $pK_a$  predictions and Marvin is shown in Fig. S5,<sup>†</sup> showing that AIBL performs very well in this respect. Roy's criteria for MAE evaluation cannot be applied here because the test set contains less than 10 compounds.

## 4. Discussion

### 4.1 Pr-BSA (S1 and TS1)

Now that we have presented the results of model construction and validation, we may take this opportunity to analyse the nature of the AIBL- $pK_a$  relationships derived here, starting with the Pr-BSA series we label “S1”. Breneman and Weber<sup>60</sup> have previously studied the charge and energy redistribution of sulfonamide ( $\text{HSO}_2\text{NH}_2$ ) and fluorosulfonamide ( $\text{FSO}_2\text{NH}_2$ ) molecules as they undergo conformational change. At a modest level of theory [HF/6-31G(d)], the authors analyzed the charge and energy of the sulfur atom and amine group of these two species during rotation around each of their interlinking S–N bond. For fluorosulfonamide, the global minimum geometry is found to be analogous to the one that we label *anti* in this work (which is used in models and predictions), whereas sulfonamide prefers to adopt the *syn* conformer. This means that in fluorosulfonamide the lone pair on nitrogen sits adjacent to the S–F  $\sigma^*$  antibonding orbital, whereas in sulfonamide the lone pair is *syn* to the S–H bond, but *anti* to the vector sum of the S–O bonds.

We may build on the work of Breneman and Weber to begin to understand the patterns of bond length variation between our series of congeners. Significantly, the authors note that the S–N bond length of fluorosulfonamide is *shorter* than that of sulfonamide (at each increment of the rotation). The authors attribute this shortening effect to the increased  $sp^2$  character of the fluorosulfonamide amine group compared to that of

sulfonamide, which instead has more  $sp^3$  character. The authors claim that as the N lone pair is donated towards the sulfur (and partially into the S–F  $\sigma^*$  antibonding orbital), this in turn, enhances the electronegativity of the N atom. Subsequently,  $\sigma$ -withdrawal of electron density occurs from the sulfur atom towards the now more electronegative N atom. This hypothesis is in part evidenced by those authors' observation that, in the *syn* conformation of fluorosulfonamide, the nitrogen of the amino group is at its peak electron population, whereas sulfur is at its most depleted. In the parlance of the authors, the fluorine atom provides a better *electron sink*, stabilising the *anti*-conformation in fluorosulfonamide *via* delocalization of the lone pair on nitrogen into the S–F  $\sigma^*$  antibonding orbital. In the absence of the F atom, the sulfonamide system favours the *syn*-conformation, due to the stabilization afforded by lone pair donation to the S–O  $\sigma^*$  antibonding orbitals over the higher energy S–H  $\sigma^*$  orbital.

Now we may consider the above rationale in the context of the S1 series, which are most stable in the *anti*-conformation. The most acidic compound of the set is S1-19 (the 2,3,4,5,6-F<sub>5</sub> derivative). In addition to having the lowest  $pK_a$  value, this compound is found to have the longest C–S (a) bond length and the shortest b–f bond length of the whole series. Fig. 9 illustrates the overall pattern of bond length variation with  $pK_a$  in terms of positive or negative correlation (shown in red or blue in Fig. 9a and in Table S17<sup>†</sup>). One interpretation of this variation in bond distances is related to the fact that the *ipso* carbon of the phenyl group in S1-19 will be more electron-poor compared to the unsubstituted analogue S1-1. It follows that the C–S  $\sigma^*$  antibonding orbital would be a better *electron sink* in S1-19 than in the unsubstituted species S1-1, making rehybridization of the N lone pair more favourable (Fig. 9b to c). Consequently, in line with the above rationale, the S–N bonding distance is shorter in species with more electron-withdrawing substituents due a *relative* increase in its *s* character. Greater *s* character of the sulfonamide N atom then in turn explains why compounds with shorter N–H (e and f) bonds have lower  $pK_a$  values: enhanced *s* character suggests that the electrons of the anion lone pair are held closer to the nucleus, thus providing enhanced stabilization to the anionic state.

In accordance with the above hypothesis, the reduction in S–N bond length will be accompanied by an increase in the C–S bond length, as electron density is put into the  $\sigma^*$  antibonding orbital, decreasing bond order. Indeed, the C–S bond length vs.  $pK_a$  plot has a negative slope, showing that congeners with the highest  $pK_a$  values have the longest CS distances (Fig. 9a).

To add further credence to the link between bond distances and  $pK_a$ , an Interacting Quantum Atoms (IQA) analysis was performed on the wavefunctions of compounds S1-1, S1-4 and S1-9, representing the unsubstituted species, the most basic (4-NHCH<sub>3</sub>,  $pK_a = 11.00$ ) and one of the most acidic compounds. Due to the close proximity in space between an *ortho* substituent and the ionizable group, S1-9 was chosen as the more acidic species over S1-19 in order to restrict substituent effects to those transmitted through bonds of the aromatic ring. The inter-atomic  $V_{\text{cl}}(\text{A},\text{B})$  values derived from IQA analysis can be interpreted as a more negative value denoting a more



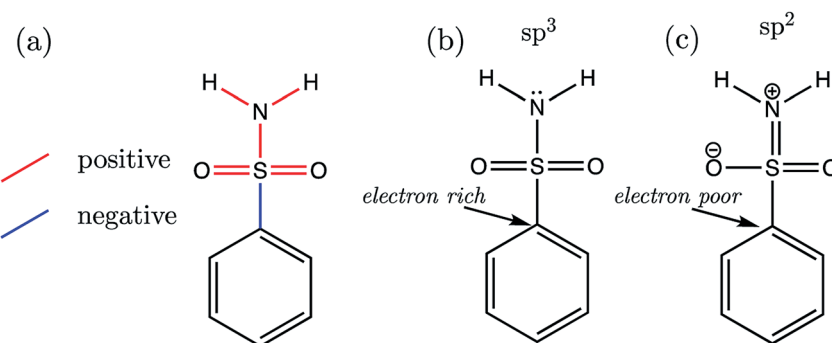


Fig. 9 (a) The structure of the common skeleton of the primary benzene sulfonamide series AP-BSA (where substituent variation occurs on the Ph ring), with bonds labelled in red (+) or blue (−) depending on the sign of the slope when regressed against  $\text{p}K_a$ . (b) The favoured  $\text{sp}^3$ -like state of the amine group under the influence of substituents, which decrease *ipso* carbon electron density. (c) The favoured  $\text{sp}^2$ -like state of the amine group under the influence of substituents, which increase *ipso* carbon electron density.

favourable electrostatic interaction. For the three species, **S1-1**, **S1-4** and **S1-9**, we find that the trend in the magnitude of  $V_{\text{cl}}(\text{A},\text{B})$  values mirrors that of the bond lengths, *i.e.* the lower the  $\text{p}K_a$ , the shorter the bond and the more negative the  $V_{\text{cl}}(\text{A},\text{B})$  value is (values are listed in Table S23†). Similarly, the exchange-correlation energy terms  $V_{\text{xc}}(\text{A},\text{B})$ , which represent the degree of electron delocalization (or *covalency*) of an interaction, also mirror the trends in bond lengths with  $\text{p}K_a$  (a more negative  $V_{\text{xc}}(\text{A},\text{B})$  value corresponds to a shorter bond A–B), except in the case of both sets of  $V_{\text{xc}}(\text{N},\text{H})$  values. For both N–H bonds, the extent of electron delocalization *decreases* between N and H atoms with *increased* acidity (*i.e.* absolute value of  $V_{\text{xc}}(\text{N},\text{H})$  decreases from 334 kJ mol<sup>−1</sup> in **S1-4** to 329 kJ mol<sup>−1</sup> in **S1-9**), whilst simultaneously, the electrostatic interaction between N and H atoms *increases* with acidity (*i.e.* the absolute value of  $V_{\text{cl}}(\text{N},\text{H})$  increases from 206 kJ mol<sup>−1</sup> in **S1-4** to 228 kJ mol<sup>−1</sup> in **S1-9**). These observations suggest that, as the N atom gains *s* character in going from  $\text{sp}^3$  to  $\text{sp}^2$  hybridization (Fig. 9a and b), there is a decrease in electron delocalization between N and H atoms, which is in line with an increased propensity for N–H cleavage.

#### 4.2 AP-BSA (S2 and TS2)

For the AP-BSA series we can rationalize the variation in bond lengths (shown in Fig. 10a) with  $\text{p}K_a$  by considering the effect of substituent groups on the *N*-phenyl ring. Firstly, it can be asserted that each substituent will affect the relative propensity of  $\pi$ -donation from the sulfonamide nitrogen into the *N*-phenyl group, akin to that described earlier for aniline derivatives (Section 3.4). A substituent *X* causing a decrease in electron density at the *ipso* carbon of the *N*-phenyl group promotes conjugation of the sulfonamide nitrogen lone pair into the aromatic ring. This effect is illustrated in Fig. 10b. Therefore, a substituent group causing the *ipso* carbon of *N*-phenyl to become more electron-poor will result in a *relatively* larger contribution from a resonance canonical with C=N (bond vi in Fig. 6a) double bond character. Whilst the sulfonamide nitrogen lone pair is partaking in conjugation with the *N*-phenyl ring, there is a lesser contribution from a resonance structure with S=N (iv) in

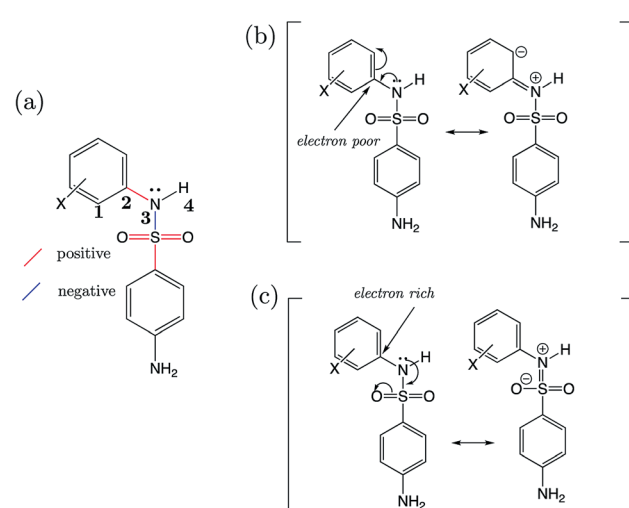


Fig. 10 (a) The structure of 4-amino-*N*-phenylbenzenesulfonamides, with bonds labelled in red or blue depending on the sign of the slope when regressed against  $\text{p}K_a$ . Atoms are numbered to illustrate the  $\text{C}^1-\text{C}^2-\text{N}^3-\text{H}^4$  torsional angle. (b) Proposed dominant resonance canonicals for the most acidic, and (c) most basic 4-amino-*N*-phenylbenzenesulfonamide derivatives of the S2 series.

bond character, because the lone pair is instead donated towards the  $\text{SO}_2$  moiety. Substituents on the *N*-phenyl ring causing the *ipso* carbon to be electron-rich cause the opposite effects on bonds C=N (vi) and S=N (iv), which is illustrated in Fig. 10c.

Support for the above rationale can be found in the observed increase in the  $\text{C}^1-\text{C}^2-\text{N}^3-\text{H}^4$  dihedral angle towards 180° (*i.e.* co-planarity of the N–H moiety with the *N*-phenyl ring), the more strongly electron-withdrawing the substituents are and the lower the  $\text{p}K_a$ . The variation in this torsional angle can be explained by an increase in  $\text{sp}^2$  character of the sulfonamide nitrogen as the lone pair is conjugated with the  $\pi$ -system, towards a quinoid-type resonance structure (Fig. 10b).

#### 4.3 SU and TSU

By reducing the set to only the 18 *n*-butyl derivatives (**SU-1** to **SU-18**), we can restrict the variation in substituent effects to the

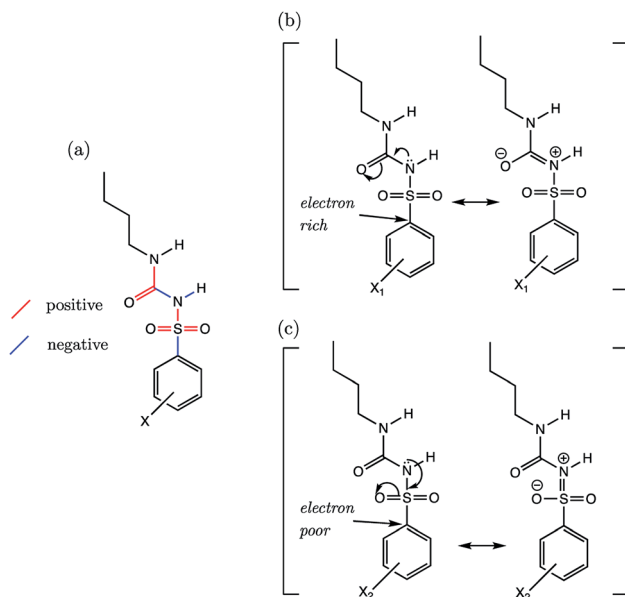


Fig. 11 (a) The signs of the slopes of bond length vs.  $pK_a$  for *n*-butylsulfonylureas substituted at the phenyl group, where red denotes a positive slope, and blue denotes a negative slope. (b) The proposed dominant resonance canonical for the most basic, and for (c) the most acidic species of the SU series.

phenyl group. In doing so,  $r^2$  values of all AIBL- $pK_a$  models (except for N–H aka (I)) lie above 0.8, demonstrative of a good linear fit (shown in Table S24†). For the sulfonylurea group, the direction of variation of C–S (A), S=O (B), S=O (C), and S–N (D) bond distances (Fig. 11a) with aqueous  $pK_a$  values mirrors that of the analogous bonds found in the primary benzene sulfonamide series S1 (Fig. 9a).

Using a similar rationale as for the benzene sulfonamides, we can assert that when the substituent  $X$  on the Ph group makes the *ipso* carbon electron-rich, the C–S  $\sigma^*$  antibonding orbital a worse *electron sink* (Fig. 11b). When the  $X$  substituent on the Ph group causes the *ipso* carbon becomes electron-poor (Fig. 11c), it becomes more stabilising to put electron density into the C–S  $\sigma^*$  antibonding orbital, and thus it is a better electron sink. In this latter case, the shortening effect on the S–N bond and the lengthening of the C–S bond would be enhanced. However, with a more electron-rich sulfur, the lone pair on nitrogen can instead be delocalized across the N–C (F) and C=O (G) bonds of the urea fragment. This direction of delocalization being favoured would explain why in the most basic compound of the series (SU-5, 4-NMe<sub>2</sub>,  $pK_a$  = 5.85), which contains a good  $\pi$ -electron donating group, the C–S (A) and N–C (F) bonds are also the shortest. The C=O bond (G) of the urea moiety in SU-5 is also the longest, suggestive of a situation similar to that shown in Fig. 10b.

## 5. Conclusions

We have demonstrated for the first time that highly correlated linear relationships exist between equilibrium bond lengths and aqueous  $pK_a$  values for three pharmaceutically relevant

variants of the sulfonamide group. For primary benzene sulfonamides, the active bond, *i.e.* the bonding distance that shows the strongest linear relationship with  $pK_a$ , is the S–N bond ( $r^2 = 0.95$ ,  $q^2 = 0.94$  and RMSEE = 0.14), where  $N$  is the site of ionization. For the secondary sulfonamide groups of 4-amino-*N*-phenylbenzenesulfonamides, the C–S bond lengths can be used to predict the  $pK_a$  ( $r^2 = 0.96$ ,  $q^2 = 0.95$  and RMSEE = 0.23). Finally, for phenylsulfonylureas, the S–N bond adjacent to the site of ionization is most highly correlated ( $r^2 = 0.93$ ,  $q^2 = 0.93$  and RMSEE = 0.14).

For the first time in the context of the AIBL approach, we have also proposed rationales for bond length variation in the presence of substituent groups, and why this may be related to their propensity to ionize.

A significant feature of the work is that we have shown that the AIBL approach may be applied to predict  $pK_a$  values of compounds with more than one ionizable group. This feat is achieved by optimization of the compound with the  $pK_{a(1)}$  site in its dissociated, anionic state. Prediction accuracy is found to be optimized by adding diffuse functions to non-hydrogen atoms [6-311+G(d,p)]. In our workflow, quantum chemical calculations are performed on only the relevant microstate, yet the average absolute error on our predictions is 0.16 log units. The overall accuracy of the AIBL predictions presented here is found to be superior to that provided by Marvin for the same series of compounds.

Finally, we have corrected the experimental aqueous  $pK_a$  values of three drug compounds: celecoxib, glimepiride and glipizide. For celecoxib, our model predicted a value of 9.72 for the sulfonamide group, which is lower by 1.58 log units than the widely quoted literature value of 11.1. The  $pK_a$  was measured once more in this work, which returned a value only 0.2 pH units away from our predicted value (9.52). Furthermore, our prediction of 5.58 for glimepiride was corroborated by a new experimental value of 5.32. Both of these new glimepiride  $pK_a$  values suggest that a significantly higher proportion of molecules exist in their anionic state at pH 7.4 than is suggested by the previously reported value (7.26). The  $pK_a$  value of glipizide was also re-measured, and the new value of 5.21 was found to be closer to our predicted value of 5.07 than the existing literature value (5.90). Moreover, glimepiride and glipizide both contain more than 50 atoms, which would invoke significant CPU time in a conventional first-principles workflow. However, we perform a quantum chemical calculation on only the neutral species, and arrive at accurate predictions despite the significant size and complexity of these compounds.

In the lead optimization process of drug discovery, we propose that AIBL can serve as a highly accurate estimator of  $pK_a$  variation for various series of analogues generated for an active scaffold. Furthermore, the AIBL- $pK_a$  approach can be used to check the consistency of a group of  $pK_a$  measurements, and can therefore serve as a rectifier for experimental outliers.

## Conflicts of interest

The authors declare no competing financial interests.



## Acknowledgements

P. L. A. P. thanks the EPSRC for Fellowship funding (EP/K005472) while P. L. A. P and B. A. C. thank the BBSRC for funding her PhD studentship under the “iCASE” award BB/L016788/1 (with a contribution from Syngenta Ltd) and for funding a subsequent postdoc with Impact Acceleration funding (IAA\_105) (with a contribution of Lhasa Ltd).

## References

- 1 E. Hansen, E. Limé, P.-O. Norrby and O. Wiest, *J. Phys. Chem. A*, 2016, **120**, 3677–3682.
- 2 H.-X. Dai, A. F. Stepan, M. S. Plummer, Y.-H. Zhang and J.-Q. Yu, *J. Am. Chem. Soc.*, 2011, **133**, 7222–7228.
- 3 S. Z. Fisher, M. Aggarwal, A. Y. Kovalevsky, D. N. Silverman and R. McKenna, *J. Am. Chem. Soc.*, 2012, **134**, 14726–14729.
- 4 T. Saha, M. S. Hossain, D. Saha, M. Lahiri and P. Talukdar, *J. Am. Chem. Soc.*, 2016, **138**, 7558–7567.
- 5 T. Uehara, Y. Minoshima, K. Sagane, N. H. Sugi, K. O. Mitsuhashi, N. Yamamoto, H. Kamiyama, K. Takahashi, Y. Kotake, M. Uesugi, A. Yokoi, A. Inoue, T. Yoshida, M. Mabuchi, A. Tanaka and T. Owa, *Nat. Chem. Biol.*, 2017, **13**, 675–680.
- 6 P. Beck, M. Reboud-Ravaux and M. Groll, *Angew. Chem., Int. Ed.*, 2015, **54**, 11275–11278.
- 7 Y. Chen, P. R. D. Murray, A. T. Davies and M. C. Willis, *J. Am. Chem. Soc.*, 2018, **140**, 8781–8787.
- 8 J. R. DeBergh, N. Niljianskul and S. L. Buchwald, *J. Am. Chem. Soc.*, 2013, **135**, 10638–10641.
- 9 F. Shi, M. K. Tse, S. Zhou, M.-M. Pohl, J. Radnik, S. Hübner, K. Jähnisch, A. Brücker and M. Beller, *J. Am. Chem. Soc.*, 2009, **131**, 1775–1779.
- 10 A. B. A. Boxall, P. Blackwell, R. Cavallo, P. Kay and J. Tolls, *Toxicol. Lett.*, 2002, **131**, 19–28.
- 11 Y. Hu, X. Yan, Y. Shen, M. Di and J. Wang, *Ecotoxicol. Environ. Saf.*, 2018, **157**, 150–158.
- 12 X. Hu, Q. Zhou and Y. Luo, *Environ. Pollut.*, 2010, **158**, 2992–2998.
- 13 A. Klamt, F. Eckert, M. Diedenhofen and M. E. Beck, *J. Phys. Chem. A*, 2003, **107**, 9380–9386.
- 14 H. Lu, X. Chen and C. G. Zhan, *J. Phys. Chem. B*, 2007, **111**, 10599–10605.
- 15 S. Zhang, J. Baker and P. Pulay, *J. Phys. Chem. A*, 2010, **114**, 425–431.
- 16 F. Eckert, M. Diedenhofen and A. Klamt, *Molecular Physics*, 2010, **108**, 229–241.
- 17 J. Ho and M. L. Coote, *Wiley Interdiscip. Rev.: Comput. Mol. Sci.*, 2011, **1**, 649–660.
- 18 J. Jensen, C. J. Swain and L. Olsen, *J. Phys. Chem. A*, 2017, **121**, 699–707.
- 19 A. D. Bochevarov, M. A. Watson and J. R. Greenwood, *J. Chem. Theory Comput.*, 2016, **12**, 6001–6019.
- 20 D. M. Philipp, M. A. Watson, H. S. Yu, T. B. Steinbrecher and A. D. Bochevarov, *Int. J. Quantum Chem.*, 2017, **118**, 1–8.
- 21 MARVIN, <http://www.chemaxon.com>.
- 22 Epik, <http://www.schrodinger.com>.
- 23 ACD Labs, <https://www.acdlabs.com>.
- 24 M. Li, H. Zhang, B. Chen, Y. Wu and L. Guan, *Sci. Rep.*, 2018, **8**, 3991.
- 25 M. Goodarzi, M. P. Freitas, C. H. Wu and P. R. Duchowicz, *Chemom. Intell. Lab. Syst.*, 2010, **101**, 102–109.
- 26 Y. Connolly Martin, *Drug Discovery Today: Technologies*, 2018.
- 27 Y. Connolly Martin, *J. Comput.-Aided Mol. Des.*, 2009, **23**, 693–704.
- 28 A. P. Harding and P. L. A. Popelier, *Phys. Chem. Chem. Phys.*, 2011, **13**, 11264–11282.
- 29 I. Alkorta, M. Z. Griffiths and P. L. A. Popelier, *J. Phys. Org. Chem.*, 2013, **26**, 791–796.
- 30 M. Z. Griffiths, I. Alkorta and P. L. A. Popelier, *Mol. Inf.*, 2013, **32**, 363–376.
- 31 C. Anstöter, B. A. Caine and P. L. A. Popelier, *J. Chem. Inf. Model.*, 2016, **56**, 471–483.
- 32 C. Dardonville, B. A. Caine, M. N. de la Fuente, G. M. Herranz, B. C. Mariblanca and P. L. A. Popelier, *New J. Chem.*, 2017, **41**, 11016–11028.
- 33 B. A. Caine, C. Dardonville and P. L. A. Popelier, *ACS Omega*, 2018, **3**, 3835–3850.
- 34 SIMCA-P 10.0, UMETRICS, Umeå, Sweden, 2002.
- 35 K. Roy, R. N. Das, P. Ambure and R. B. Aher, *Chemom. Intell. Lab. Syst.*, 2016, **152**, 18–33.
- 36 M. A. Blanco, A. Martín Pendás and E. Francisco, *J. Chem. Theory Comput.*, 2005, **1**, 1096–1109.
- 37 M. Remko and C.-W. von der Lieth, *Bioorg. Med. Chem.*, 2004, **12**, 5395–5403.
- 38 M. Remko, *J. Mol. Struct.: THEOCHEM*, 2010, **944**, 34–42.
- 39 V. Petrov, V. Petrova, G. V. Girichev, H. Oberhammer, N. I. Giricheva and S. Ivanov, *J. Org. Chem.*, 2006, **71**, 2952–2956.
- 40 S. K. Paulson, M. B. Vaughn, S. M. Jessen, Y. Lawal, C. J. Gresk, B. Yan, T. J. Maziasz, C. S. Cook and A. Karim, *J. Pharmacol. Exp. Ther.*, 2001, **297**, 638–645.
- 41 S. Goto, Y. Odawara, M. Nakano and Y. Araki, *Yakugaku Zasshi*, 1978, **98**, 236–241.
- 42 T. Takayangi, M. Isoda, D. Itoh and H. Mizuguchi, *Bunseki Kagaku*, 2017, **99**, 509–514.
- 43 B. Song, A. K. Galande, K. Kodukula, W. H. Moos and S. M. Miller, *Drug Dev. Res.*, 2011, **72**, 416–426.
- 44 H. Wan, A. G. Holman, Y. Wang, W. Lindberg, M. Englund, M. B. Nagard and R. A. Thompson, *Rapid Commun. Mass Spectrom.*, 2003, **17**, 2639–2648.
- 45 M. Manderscheid and T. Eichinger, *J. Chromatogr. Sci.*, 2003, **41**, 323–326.
- 46 S. S. Chourasiya, D. R. Patel, C. M. Nagaraja, A. K. Chakraborti and P. V. Bharatam, *New J. Chem.*, 2017, **41**, 8118–8129.
- 47 P. Deprez, B. Heckmann and A. Corbier, *Bioorg. Med. Chem. Lett.*, 1995, **5**, 2605–2610.
- 48 F. Mohamadi, M. M. Spees and G. B. Grindey, *J. Med. Chem.*, 1992, **35**, 3012–3016.
- 49 J. Wang, Y. Xiao, Y. Li, Y. Ma and Z. Li, *Bioorg. Med. Chem.*, 2007, **15**, 374–380.
- 50 R. A. LaRossa and J. V. Schloss, *J. Biol. Chem.*, 1984, **259**, 8753–8757.



51 Y. Kasetti, N. K. Patel, S. Sundriyal and P. V. Bharatam, *J. Phys. Chem. B*, 2010, **114**, 11603–11611.

52 S. Grbic, J. Parojcic, A. Malenovic, Z. Djuric and M. Maksimovic, *J. Chem. Eng. Data*, 2010, **55**, 1368–1371.

53 S. Asada, R. Fujita and Y. Shirakura, *Yakugaku Zasshi*, 1974, **94**, 80–87.

54 S. Asada, T. Nakasato and S. Takino, *Yakugaku Zasshi*, 1973, **93**, 1647–1654.

55 H. Wan, A. G. Holman, Y. Wang, W. Lindberg, M. Englund, M. B. Nagard and R. A. Thompson, *Rapid Commun. Mass Spectrom.*, 2003, **17**, 2639–2648.

56 P. Hadju, K. F. Kohler, F. H. Schmidt and H. Spingler, *Arzneim. Forsch.*, 1969, **19**, 1381–1386.

57 R. J. Prankerd, in *Profiles of Drug Substances, Excipients, and Related Methodology*, ed. H. Brittain, Elsevier, 2007, vol. 33.

58 M. Schwanstecher, C. Schwanstecher, C. Dickel, F. Chudziak, A. Moshiri and U. Panten, *Br. J. Pharmacol.*, 1994, **113**, 903–911.

59 U. Quast, D. Stephan, S. Bieger and U. Russ, *Diabetes*, 2004, **53**(suppl 3), S156–S164.

60 C. M. Breneman and L. W. Weber, *Can. J. Chem.*, 1996, **74**, 1271–1282.

